Helmus, R., Kratz, J., Potter, K., Hubert, P., & Hinterholzl, R. (2017). An experimental technique to characterize interply void formation in unidirectional prepregs. *Journal of Composite Materials*, *51*(5), 579-591. https://doi.org/10.1177/0021998316650273

An experimental technique to characterise the interply void formation in unidirectional prepregs

R. Helmus[a], J. Kratz[b], K. Potter[b], P. Hubert[c], R. Hinterhölzl[a,*]

[a] *Institute for Carbon Composites, Technische Universität München, Faculty of Mechanical Engineering,Boltzmannstrasse 15, D-85748 Garching b. München, Germany.*
[b] *Advanced Composites Centre for Innovation and Science, University of Bristol, Queens Building, University Walk, Bristol BS8 1TR, United Kingdom.*
[c] *Department of Mechanical Engineering, McGill University, 817 Sherbrooke St. West, Montreal, Quebec, H3A 0C3, Canada.*

Abstract

Out-of-Autoclave (OoA) prepreg processing requires evacuation of volatiles at the early stages of processing to achieve an acceptable final void content. In this study, single prepreg plies were laid-up onto a glass tool to simulate a ply-ply interface to gain an understanding of initial air entrapment and eventual removal mechanisms. The contact was recorded during processing with various edge breathing configurations to identify the relationship between evacuation pathways and contact evolution. The existence of preferential flow channels along the fibre direction of the material was shown by characterising the prepreg surface. Gas evacuation in those channels prevented contact during an extended ambient temperature vacuum hold. The contact between the prepreg and glass tool equilibrated around 80% during the ambient vacuum hold, and reached full contact at elevated temperature after a brief loss in contact due to moisture vaporization when the resin pressure decreased below the water vapour pressure.

Keywords: Prepreg, Porosity, Process Monitoring, Out of autoclave processing.

*Corresponding author
Email address: hinterhoelzl@lcc.mw.tum.de (R. Hinterhölzl)

1. Introduction

Void formation in composite manufacturing remains one of the primary processing defects because it is well known that they have a detrimental effect on the mechanical properties of laminated composites [19]. Void formation in prepreg processes is usually suppressed by applying high pressures in either a press or an autoclave to dissolve volatiles into the resin. However, recent demands for more sustainable manufacturing processes, including of Out-of-autoclave (OoA) prepregs, have increased the scientific interest in void phenomena because these processes use lower pressures that cannot suppress voids to the same extent as in the autoclave process. Lower consolidation pressure during vacuum-bag-only processing of OoA prepregs may be accompanied by an enhanced susceptibility to porosity.

In order to produce void free parts, processing parameters have to be chosen carefully, based on a thorough understanding of void formation. Furthermore, a special prepreg microstructure is required to enhance gas evacuation prior to cure. OoA prepregs are initially partly impregnated, consisting of a dry central fibrebed surrounded by resin rich areas [2]. Before heating and during the early stages of the cure cycle, the dry areas form permeable channels that allow gas evacuation. As heating begins, the dry microstructure is infiltrated by the softening epoxy resin from the resin rich areas. Full prepreg impregnation is desired before gelation, but concurrently, if evacuation channels remain permeable in the early heating stages they offer residual volatiles extraction opportunities [21].

Various void generation and dissipation mechanisms will contribute to void formation during processing based on the initial material structure, handling, lay-up, and processing parameters. A general classification of voids has identified three major types [5]: intraply voids within a single fibre layer, resin voids, and interply voids between adjacent plies. Intraply voids are initially caused by insufficient impregnation of the dry areas within the OoA prepreg

structure. These voids will remain in the finished laminate if the resin content is insufficient, the resin viscosity profile does not allow full wetting of the dry fire regions, or the resin pressure is insufficient during processing. Resin voids are induced during the prepregging process or during the cure reaction as volatiles are released, or moisture is diffused out of the resin. Both intraply and resin voids have been addressed in previous studies [8, 3, 14, 23]. Interply voids between layers are caused by mechanical entrapment of air pockets during ply deposition. Material factors contributing to the initial interply air entrapment and distribution include ply surface topology and premature contact to the opposing surface due to tackiness [10]. Additional geometrical or processing entrapment factors during lay-up include ply terminations, material handling, lay-up conditions (temperature and humidity), and contamination. Geometrical and processing factors are more difficult to capture than material factors, but regardless of their origin, once entrapped between plies, isolated air pockets will remain as interply voids within the final part if they cannot be removed or consolidated during the manufacturing process.
The literature covering interply void formation in the OoA process is still very limited compared to what is known about resin and intraply void formation. To date, woven fabrics have been the primary focus of interply void research, and they initially represent the greatest fraction of total void content [5]. These voids generally decrease to zero during processing, which is attributed to air evacuation through gaps created by the interlaced structure. The same phenomena cannot be transferred to unidirectional prepregs, due to smoother surfaces compared to woven prepregs, as well as lower out-of-plane air permeability [16].
In-situ experimental techniques to characterise interply void formation are currently limited. Micro-CT would be the ideal tool to capture the three dimensional evolution of interply voids during processing, but the current scan times are too slow to capture the temporal change during the initial vacuum application and scan resolutions needed to capture the spatial distribution of interply voids are limited to small sample sizes. Since the interply void for-

mation mechanisms resemble the entrapment and evacuation of air between a tool-ply interface, a glass plate and optical camera may offer the speed and resolution to monitor void evolution in processing conditions. Replicating a multiple prepreg ply-ply interface in a laminate by a single ply applied to a rigid mould will likely change the boundary conditions in this region of interest. The contact mechanics between the resin at the tool-ply interface will likely differ to those of an isolated bubble surrounded by resin. Additionally, the complex nature of transverse compaction stresses transferred at different angles through ply nesting may influence the contact and air flow pathways. Clearly, this technique is not without limitations, but it can offer qualitative insights to capture the void evolution in different processing conditions in relevant time intervals.

The transparent mould approach has been used by Bloom et al. [1] to study the effect of ply consolidation of different ply deposition techniques, such as hand lay-up and roller assisted methods, and the influence of flexible bagging consumables on the applied pressure distribution in prepreg processing. In a separate study, Hamill et al. [10], also used a glass plate and camera to investigate the influence of material and processing parameters on surface porosity, and identified air entrapment as the primary source of large surface pores after cure. Additional information about the height of the void can be obtained by surface roughness measurements. Lukaszewicz and Potter measured the surface roughness of uncured autoclave and OoA fibre placement grade prepreg tapes [18], and they concluded that rougher prepreg surfaces will influence the cured laminate interply void content.

In light of the fact that interply voids contribute to the degradation of mechanical properties, coupled with a shift towards low pressure processing, a need exists to capture the initial distribution of these voids and describe how they evolve during processing in order to understand which gas evacuation mechanisms are available to minimise cured part porosity. In this study, the surface roughness of an OoA prepreg was studied to evaluate the texture and properties of the material in its uncured state to inform void

formation in a unidirectional prepreg. This characterisation was followed by measuring the contact evolution of the OoA prepreg ply on a glass tool using different in-plane breathing configurations. The images were post-processed to determine if the contact mechanisms changed during ambient and elevated temperature processing to understand the air evacuation mechanisms of interply voids during OoA prepreg consolidation.

2. Material constitution

OoA prepreg materials are supplied partly impregnated, consisting of dry fibre and resin rich areas that will ideally become void free after elevated temperature curing. Fig. 1 shows an example of a post-processed CT image of an uncured *Cytec Engineered Materials' Cycom® 5320* OoA prepreg microstructure; this image was generated using the procedure outlined in [12]. The carbon fibre prepreg, with a fibre density of $1.77\,\frac{g}{cm^3}$, was supplied with an epoxy resin that accounts for roughly 33 weight% of the material. This particular prepreg was supplied with a relatively stiff single-sided paper backing. The prepreg is a vacuum bag only curable prepreg allowing a curing temperature of either 93 °C or 121 °C, according to the manufacturer's data sheet. Even though prepregs are machine made by a commercial process,

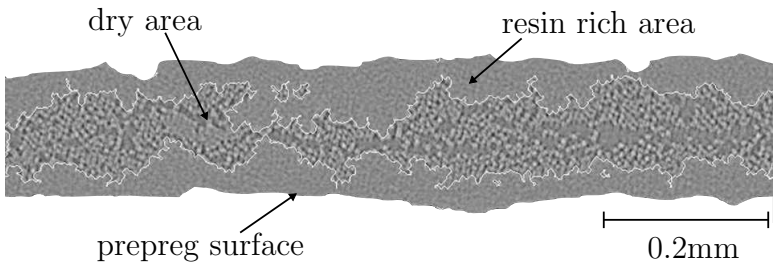

Figure 1: CT image of an uncured UD prepreg's cross-section.

Fig. 1 reveals that the prepreg material has an irregular resin distribution on the surface that can lead to variations in the cross-section of the prepreg. This induces variations in the prepreg fibre volume fraction, which in-turn

leads to variability in the in-plane air permeability. Variability in the out-of-plane permeability may also occur. A Scanning Electron Microscopy (SEM) image of the prepreg surface is shown in Fig. 2 and identifies point-to-point variations in the resin distribution that may promote local areas of higher out-of-plane air permeability compared to adjacent resin rich regions. Both

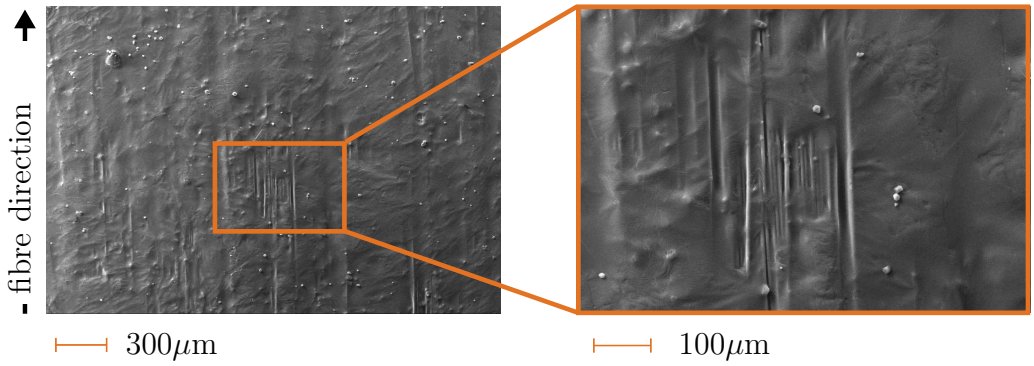

Figure 2: SEM image of a UD prepreg surface before processing.

Fig. 1 and 2 expose the rough surface of the prepreg which may not only be affected by variations in the resin distribution due to manufacturing techniques but also due to material transport, storage, and handling before final usage. For a better understanding of the surface properties, surface roughness scans were conducted using an Alicona G5 optical micro coordinate measurement system. A 50 mm × 25 mm sample was mounted to a glass slide and sputter coated with 30 nm of gold prior to scanning. The centre surface topology of a 10 mm × 10 mm region of both the backing paper and the non-backing paper side of the prepreg are shown in Fig. 3.

The maximum volume entrapped by each sides was determined by a surface scan. The void volume of the surface was subdivided into the core and valley void volumes, as shown in the cross-section of a prepreg layer in Fig. 4, using the bearing area curve. The values for each area are presented in Table 1 and indicate that there is a marked difference in surface roughness between the backing paper and non-backing paper side of the prepreg. As a result,

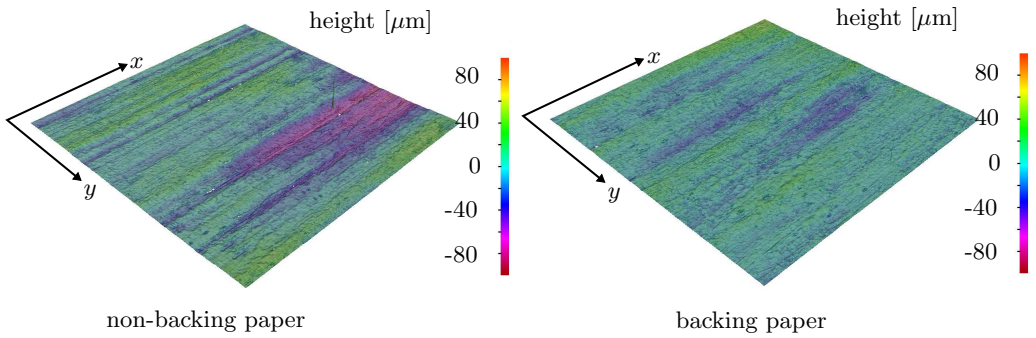

Figure 3: 10 mm × 10 mm surface of an uncured UD prepreg. Fibres are oriented in x-direction.

the non-backing paper side of the material will entrap a larger volume of air than smoother backing paper side. To capture the worst case scenario, coupled with the likely manufacturing procedure of laying-up the non-backing side of the prepreg, the non-backing side of the prepreg was placed onto the glass tool. The surface roughness of the prepreg determines both the initial

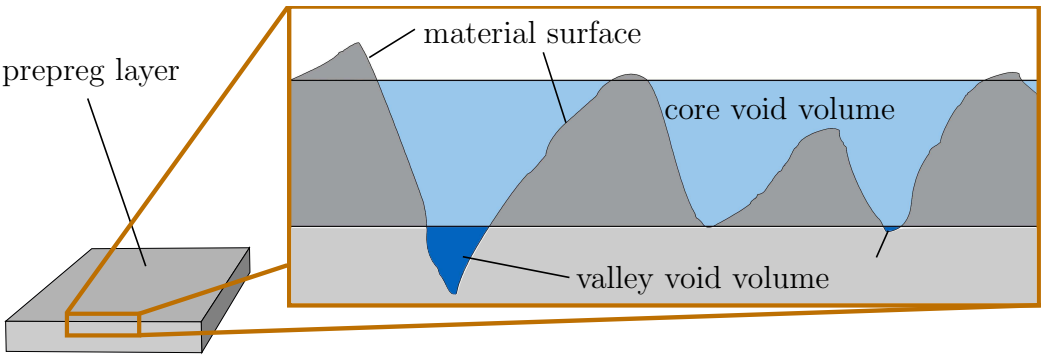

Figure 4: Cross Section of void volume depending on the surface roughness. According values in Table 1 are based on the bearing area curve (BAC) [6].

volume of entrapped air, but also the ability to evacuate air from the lay-up. A corduroy surface structure running parallel to the fibre direction generated interconnected pathways for air evacuation in the interply region until the combined compaction and evacuation collapsed this structure.

Table 1: Comparison of the prepreg's backing paper and non-backing paper surfaces. Core and valley void volume values refer to the prepreg surfaces shown in Fig. 3 and were determined using the bearing area curve [13].

Prepreg side	backing paper	non-backing paper
Core void volume	$12.5\ \frac{\mathrm{ml}}{\mathrm{m}^2}$	$24.3\ \frac{\mathrm{ml}}{\mathrm{m}^2}$
Valley void volume	$1.4\ \frac{\mathrm{ml}}{\mathrm{m}^2}$	$3.1\ \frac{\mathrm{ml}}{\mathrm{m}^2}$

As represented in Fig. 5, the interply zone (1) may not be the only evacuation possibility. Air may flow from the interply zone into the intermediate dry layer based on the pressure differential between the regions and the opposing resin viscosity. Subsequently, air can either be removed by the evacuation channels (2), remain in the intermediate layer (3), or migrate in the out-of-plane direction (4). Void compression (5) or dispersion (6) are also possible and are governed by the applied pressure. According to Persson et al. [20],

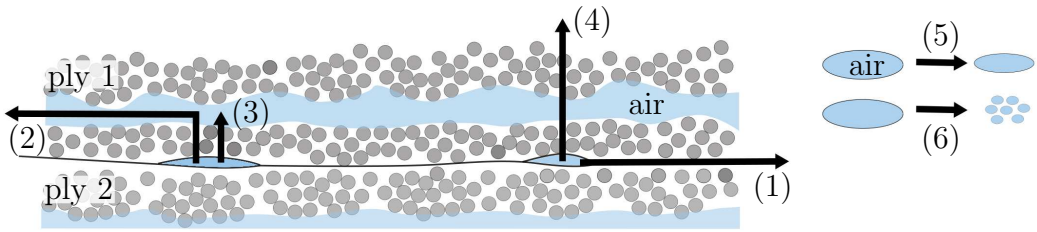

Figure 5: Interply void removal mechanisms.

the surface roughness determines the entrapped void volume and possible evacuation pathways, but has also an enormous influence on tack, which in turn has an influence on air entrapment [10]. Therefore, void spaces may remain in the interply region because the prepreg fibres will oppose bending and the high viscosity resin on the surface may not cold flow. The pressure in these void spaces will depend on the resisting gas pressure at the ply-ply interface, or whether the resin pressure can either dissolve the gas into the resin or redistribute the gas within the ply, such as the dry region within a

partially saturated prepreg.

3. Experimental approach

In this study, the contact evolution between a prepreg ply and a glass plate was recorded in order to evaluate the interply void formation. The glass surface does not have the same properties as a prepreg, but might correspond more closely to a well debulked prepreg surface and, more importantly, this technique enabled real time imaging of the contact evolution of a relatively large sample area during processing conditions.

3.1. Test Setup and Postprocessing

Multiple trials with different edge breathing conditions were carried out by laying up a single 300 mm × 300 mm prepreg ply on a 10 mm thick untreated glass tool. The prepreg plies were at the same time and stored in a freezer at −20 °C in individually sealed bags to maintain the same initial material conditions between trials. The prepreg ply was laid-up by hand and pressed against the glass tool before placing the consumables and installing the vacuum bag. The bagging arrangement consisted of a non-perforated release film, vacuum bag, four layers of breather, a 4 mm thick heater pad, 4 thermocouples, an aluminium caul sheet of 3 mm used to even out heat distribution from the heater pad and consistently apply transverse pressure to the prepreg ply in each trial, avoiding the variations in pressure encountered with a flexible membrane bag [1]. Edge breathing dams were made of sealant tape wrapped in fiberglass (unless otherwise specified) and located around the edge of the ply. A cure cycle corresponding to the manufacturer's specification was applied using a closed loop controller for the heater pad, while a vacuum port adjacent to the ply was connected to a vacuum pump. The experimental set-up is shown in Fig. 6.

A DMK 2 mega-pixel monochrome digital camera was placed underneath the glass tool to capture images during the process. Lighting conditions of

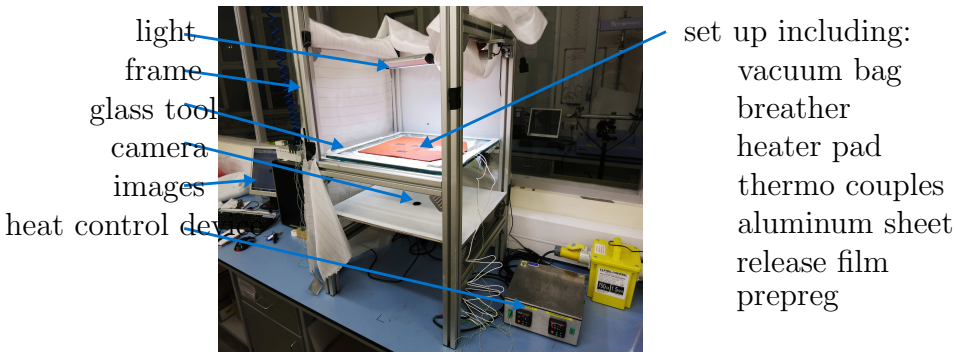

Figure 6: Glass tool set up used for contact experiments.

the images were improved by an additional light installed above the glass tool to provide the most diffuse illumination possible around the edge of the ply while avoiding reflections from placing direct lighting underneath the sample. Images were post-processed in *MATLAB*®. First, edges were cropped, reducing the raw 260 mm × 220 mm images to 210 mm × 170 mm in order to eliminate fish-eye effects at the corners. Second, an invariable threshold value was used for each sequence to convert images into binary images, consisting of black and white pixels. The contact area was determined for every image by counting the number of black pixels, excluding the circular camera reflection located in the middle of the images. The contact area was related to the total pixel count of each image, and given as a percentage.

3.2. Test matrix

To investigate the air evacuation pathways described in Fig. 5, air removal was evaluated using four different configurations. The first configuration consisted of full edge breathing placed around all four prepreg sides using edge breathing dams consisting of sealant tape wrapped in fibreglass. Out-of-plane air evacuation was restricted by a non-perforated release film (Fig. 7 (a)). In the second configuration, all four edges as well as the release film were sealed to the glass tool, restricting air to relocation or compression within the prepreg ply (Fig. 7 (b)). In the third configuration, evacuation pathways were sealed by 0.025 mm thick flash tape wrapped around the prepreg edges

to restrict gas flow to the glass tool-ply interface region (Fig. 7 (c)). Finally, edge breathing was placed on one side only, sealing the other three edges with sealant tape and closing off the surface with non-perforated release film (Fig. 7 (d)). Although similar in-plane flow should occur between the one-sided and the full edge breathing experiments, the one-sided configurations were used to determine if a contact gradient was present during evacuation. Three repeats were conducted for each boundary condition.

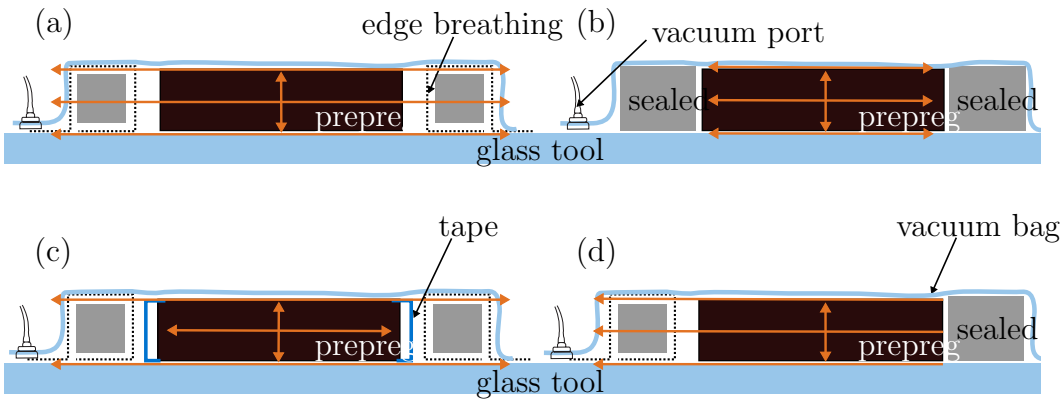

Figure 7: Four different experimental set-ups used to investigate air evacuation pathways: (a) full edge breathing, (b) sealed edges, (c) evacuation channels sealed and (d) one-sided edge breathing.

4. Results and discussion

4.1. Contact evolution over time

At the beginning of each experiment almost no contact points are present. A rapid increase in contact occurs after the vacuum was applied. Contact patterns after 10 min, 1 hour and 10 hours into the vacuum hold are presented as binary images in Fig. 8 for one repeat from each configuration. Close inspection of these images shows the temporal contact evolution. Contact initiates at random locations and then evolves from these initial contact points. Contact areas were more likely to grow from these initial points

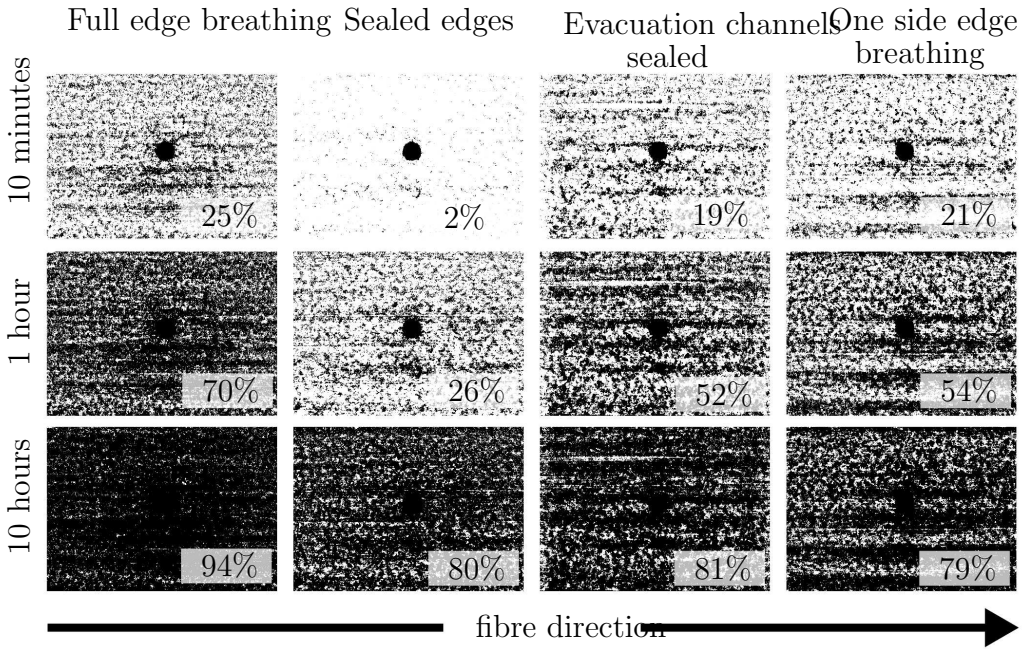

Figure 8: Percentaged contact evolution during the vacuum hold for the four edge breathing conditions - binary images (210 mm × 170 mm). Black areas indicate the contact between glass plate and prepreg, while the black circle in the centre of each image is the reflection of the camera.

rather than the smaller areas of contact preferentially growing to become connected. This offers some insight into how the entrapped air migrates in the interply region to create void spaces in the non-contact areas. Furthermore, the non-contact regions seem to stay interconnected, running parallel to the prepreg fibre direction, which remained identifiable throughout every experiment, regardless of the edge breathing configuration. Overall, these observations suggest that the non-contact areas contribute to the air evacuation in the interply region. An initial visual examination of Fig. 8 revealed no distinct difference in contact patterns between different edge breathing conditions. In order to identify if a preferential contact pattern occurred between test configurations, an amplitude density function of the mean con-

tact area along and across the fibre direction was plotted. No statistically significant difference was observed between the width of the interconnected non-contact regions.

Fig. 9 shows the contact evolution during a 12 hour ambient temperature vacuum hold for all three repeats for the four edge breathing conditions. Contact increases with time and reaches equilibrium after about 6 hours where the final contact area remains between 70% and 90% for all edge breathing conditions. The variability between trials does not allow for a clear distinction between the effect of the different edge breathing conditions on ambient evacuation mechanisms. The inconsistent and localized nature of air entrapment was also observed on the tool ply interface [10, 1] and confirms the random nature of prepreg surfaces.

After the 12 hour ambient vacuum hold, the prepreg was heated at 2 °C/min

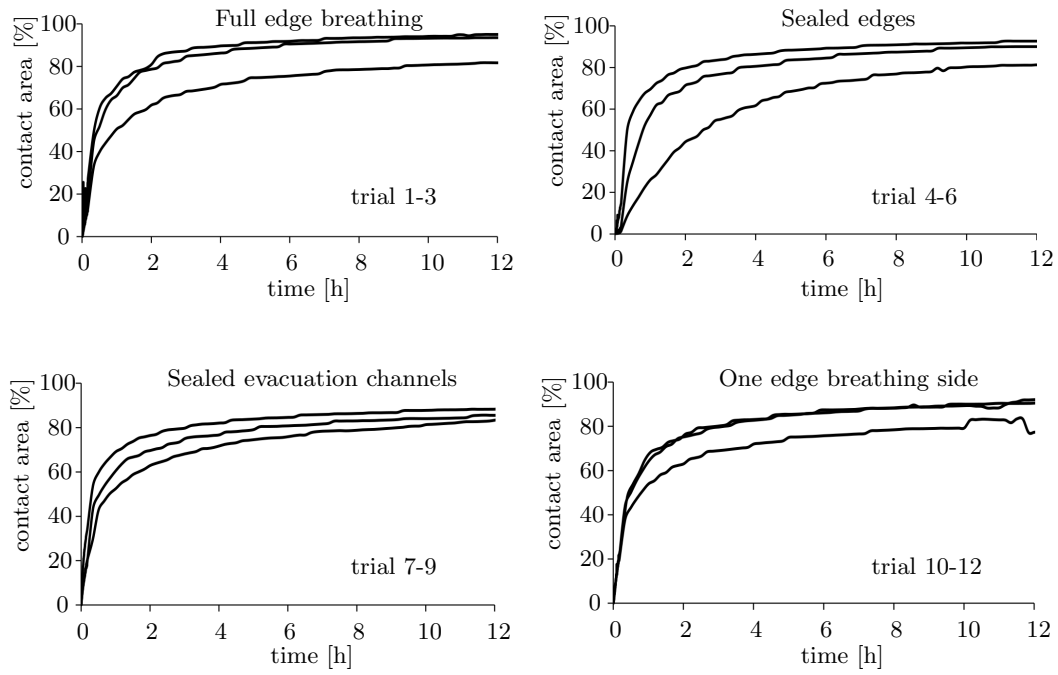

Figure 9: Contact evolution during vacuum hold for different edge breathing conditions.

to 93 °C, and the contact evolution is shown in Fig. 10. Each trial reached

full contact during the elevated temperature processing stage of the study, however, after approaching 100% contact, all configurations showed a drop in contact at around 90 °C, before eventually returning to full contact again. Moisture was considered as a possible cause of the loss in contact, therefore the effect of moisture devolution was considered by comparing estimates of the water vapour pressure to the resin pressure. If the resin pressure is higher than the water vapour pressure, moisture will remain in solution [14]. The dashed vertical line in Fig. 10 is the cross-over point where the resin pressure becomes lower than the water vapour pressure, and a loss in contact was observed.

The changes in water vapour and resin pressures during elevated tem-

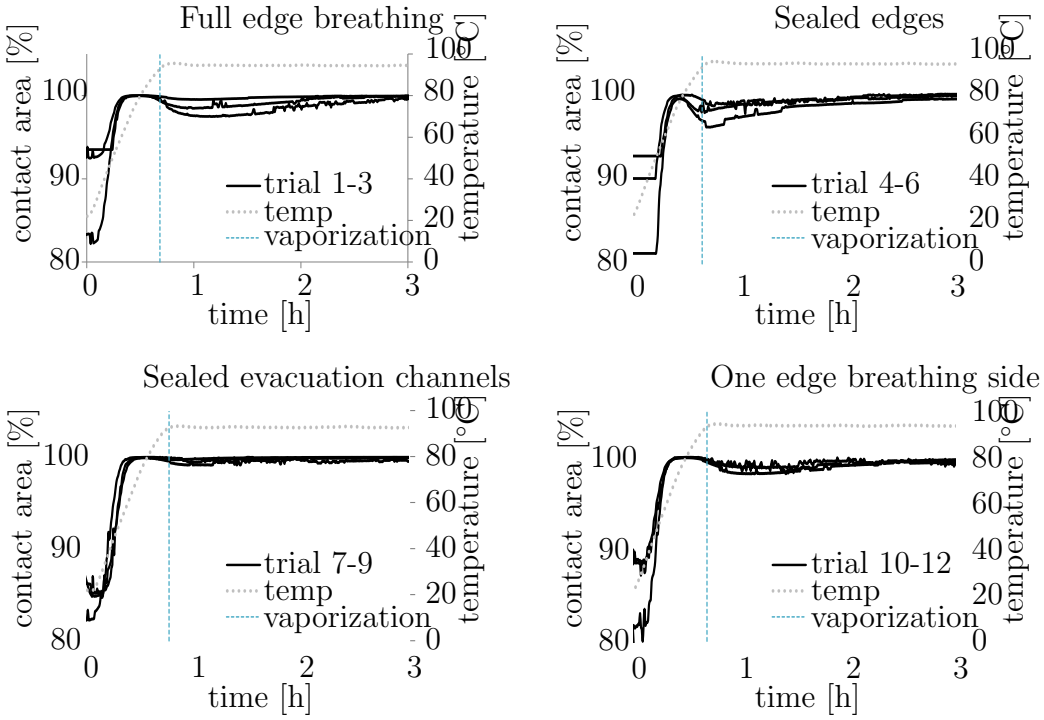

Figure 10: Contact evolution during heat application for different edge breathing conditions.

perature processing are shown in Fig. 12. The water vapour pressure was estimated by the model developed by Kardos et al. [14], which describes the

relationship between water vapour pressure, P, in bar and temperature, T, in °C:

$$P = 502774 \cdot \exp\left(\frac{-4892}{T}\right). \tag{1}$$

The resin pressure, P_r, during processing depends on the load sharing of the applied pressure, P_applied, between the resin and fibres (Fig. 11) according to

$$P_\mathrm{r} + \sigma_\mathrm{f} = P_\mathrm{applied}, \tag{2}$$

and is governed by the fibre bed compaction curve,

$$\sigma_\mathrm{f} = f(V_f) \tag{3}$$

which relates the effective stress σ_f carried by the fibre bed to the fibre volume fraction V_f [9]. The load shared between the resin and fibre regions of

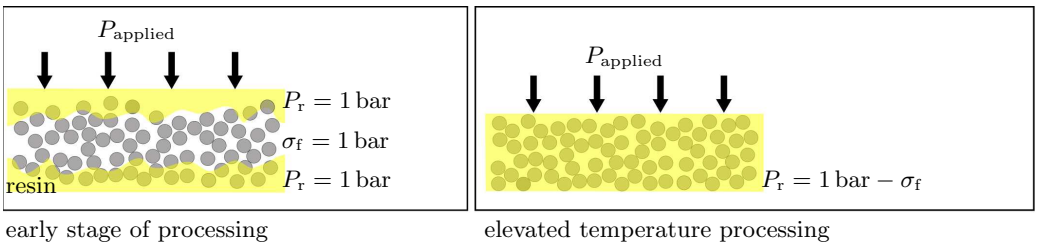

Figure 11: Load share between fibres and resin during processing where σ_f is determined by the fibrebed compaction curve.

an OoA prepreg was described by a previously developed model [11], which relates the thickness change of a prepreg to the resin flow into dry fibre areas. The initial resin pressure in OoA laminates is much higher than would be expected for autoclave prepreg processing because the partially impregnated nature of OoA materials effectively places the resin in series with the fibrebed. As the semi-solid resin film softens during elevated temperature processing, the resin saturates the fibrebed, and the applied load is shared. As a result, the resin pressure in Fig. 12 becomes constant after 1.5 hours into the heating due to the termination of the model as soon as full resin impregnation is reached. The resin pressure would be expected to decrease

as the resin shrinks after gelation [7]. However, the resin is in a pre-gelled state for the results shown in Fig. 10 and Fig. 11, therefore, the effects of chemical shrinkage are not encountered in this study.

In Fig. 12, the resin pressure exceeds the water vapour pressure at around

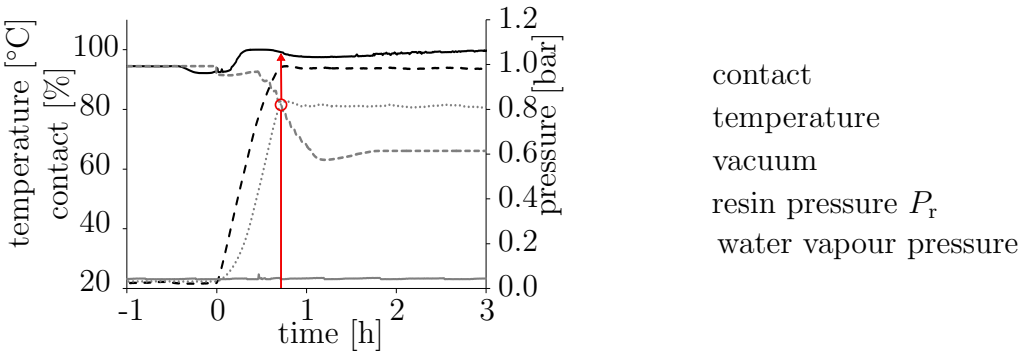

Figure 12: Water vapour and resin pressure development during heat and vacuum application compared to the contact evolution under full edge breathing conditions. The cross-over point of the water vapour and resin pressures caused a loss in contact due to moisture diffusion out of the material.

90 °C, and simultaneously, a decrease in contact between the prepreg ply and glass tool was observed. This suggests that absorbed moisture is released by the material into the interply zone, which may contribute to the drop in contact. The temperature where the water vapour and resin pressure cross-over are indicated in Fig. 10. The loss in contact in the sealed edges configuration starts earlier than the other trials in Fig. 10 because of the additional entrapped air at the tool-ply interface.

The final interply void content appears to be independent of the edge breathing conditions. This was an unexpected result, especially for the completely sealed edges configuration. Since air cannot be evacuated out of the prepreg, air removal options (1), (2) and (4) in Fig. 5 are not available, therefore air initially located in the interply region must relocate to the intraply dry area of the prepreg (3), be compressed (5), or dispersed (6).

The air initially entrapped in the interply region has likely relocated to the intraply dry area in the sealed configuration. This assumption is supported

by a quality study of OoA laminates conducted by Centea and Hubert [4]. They processed prepregs with sealed edges and when compared to laminates processed with full edge breathing, the laminates with sealed edges had an increased void content in the dry intraply area. After we processed plies with sealed edges, the removal of the cured ply from the glass tool was different compared to other configurations. Fibres that were located in the middle of the prepreg remained dry after processing and induced ply splitting during removal.

4.2. Contact evolution with temperature

The contact evolution is plotted as a function of temperature in Fig. 13 in order to analyse the relationship between temperature, resin viscosity, and ply contact. The resin viscosity was calculated by published cure kinetics and viscosity models [15]. For all four edge breathing conditions, the initial contact at room temperature stagnates between 70% to 90%. Full contact was eventually achieved in all four configurations, but contact of set-ups with breathable edges evolved almost steadily after 35 °C, whereas the contact for the sealed edge configurations remained constant up to about 50 °C. This behaviour indicates that entrapped volatiles remain at the tool-ply interface, preventing resin flow into the interply region. If the areas of non-contact were empty spaces, with an equivalent pressure to the vacuum bag, resin would flow into the non-contact areas at the same rate as the other experiments. As a result, in the sealed edge configuration air relocation cannot occur until the viscosity is sufficiently low enough to allow air flow into the intermediate layer [22, 17].

4.3. Directional contact evolution

The contact images were analysed for a spatial gradient in order to identify if the contact preferentially initiates at the edge of the ply and temporally increases towards the centre, or vice-versa. The images were subdivided into three different areas depending on the breathing configuration being tested, as shown in Fig. 14. The one-sided edge breathing trials were evaluated by

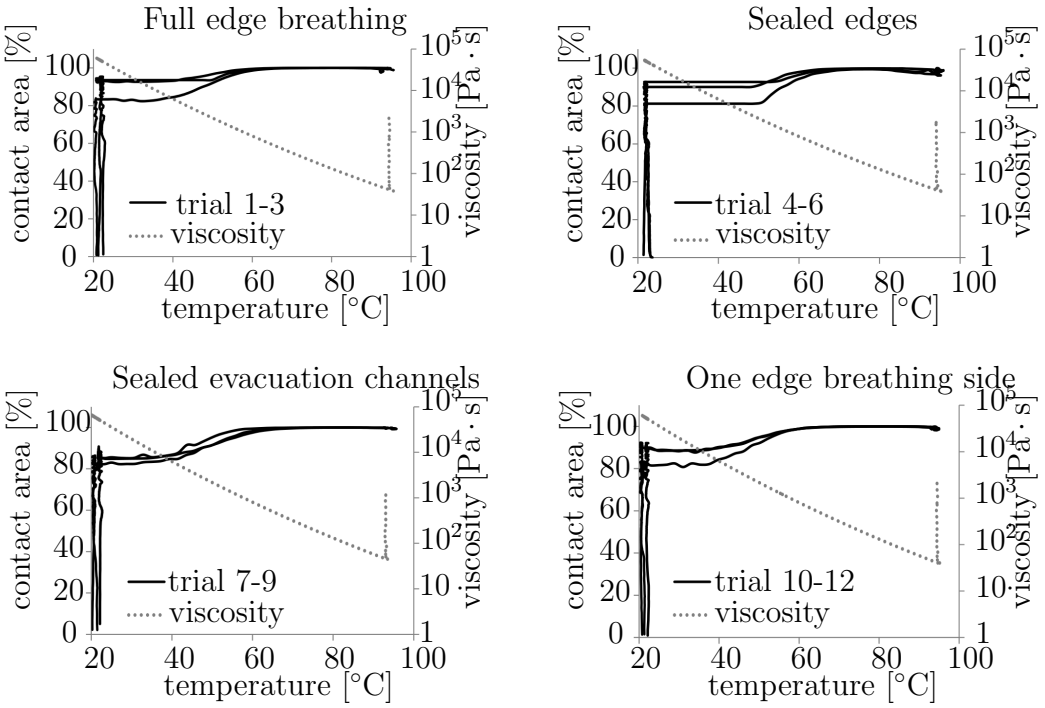

Figure 13: Contact evolution with temperature for different edge breathing conditions.

subtracting the left area from the middle area (Fig. 15(a)) and the middle area from the right area (Fig. 15(b)), according to the regions defined in Fig. 14(a). The configurations with full edge breathing were also subdivided into three regions, but the contact regions were arranged as concentric rectangles, as shown in Fig. 14 (b), since air could be extracted around all four edges of the ply. Fig. 16 depicts the difference between the outer and middle regions, and the difference between the middle and inner regions. From the analysis in Fig. 15 and Fig. 16 it appears that the ply contact evolves slower in areas close to the edge of the ply that allows air evacuation. This indicates that the non-contact areas create air evacuation pathways, which in turn inhibits contact. In the case of full edge breathing, contact evolves from the middle of the ply, whereas contact for the one-sided edge breathing initiates from the side opposite the edge breathing. Overall, contact evolved faster in the middle, but this could be related to local phenomena within the

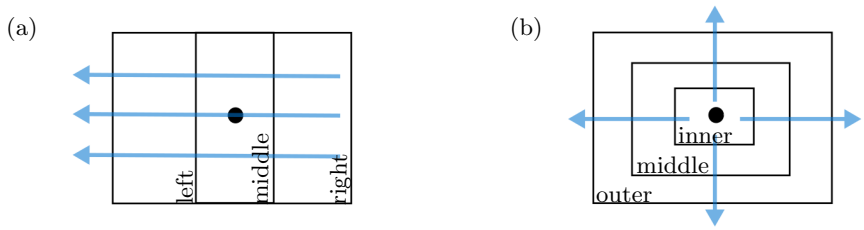

Figure 14: Areal subdivision for directional contact evolution: (a) for one-sided edge breathing tests and (b) for full edge breathing.

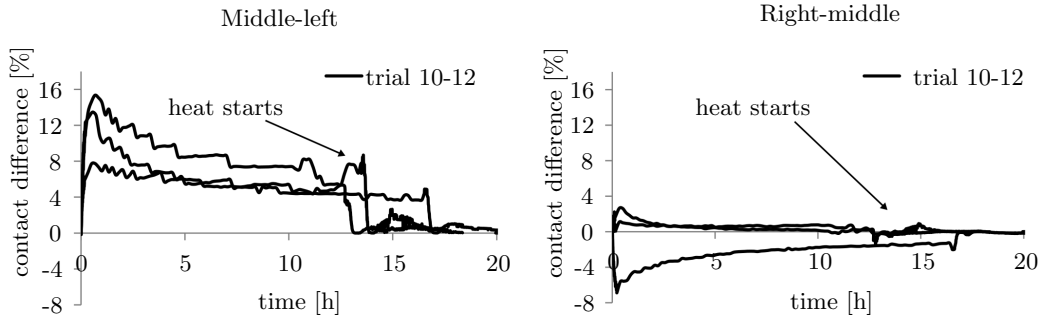

Figure 15: Gradient in contact evolution for one-sided (left) edge breathing.

ply that influence property variations. For example, variations in the surface roughness, or the in-plane and out-of-plane air permeability coefficients could influence how contact forms between the ply and the glass plate.

The linear contact gradient used in Fig. 14(a) was applied to both the one sided edge breathing and full edge breathing trials. This analysis allowed us to compare whether the contact gradient observed in Fig. 15(left) was an anomaly created by the experimental set-up. The results of this analysis are shown in Fig. 17, and confirms that the experimental set-up did not create the linear gradient because a contact gradient was always observed in the one-sided edge breathing configurations, whereas contact was observed to evolve from both sides in the full edge breathing configuration. The contact gradient disappeared as soon as heat was applied to both breathing configurations. The evacuation pattern of unidirectional OoA prepregs was evaluated

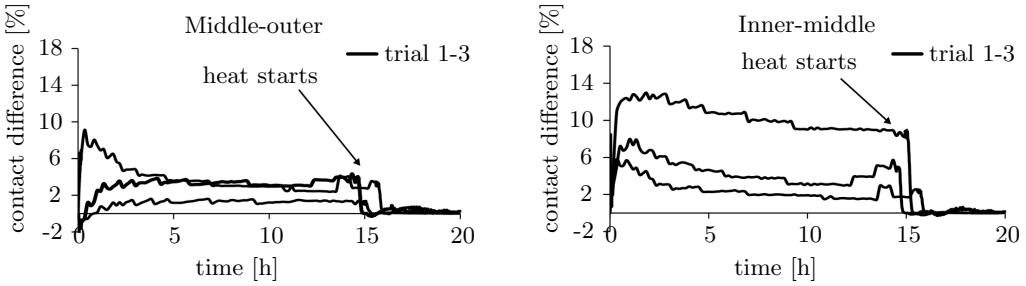

Figure 16: Contact gradient evolution for the full edge breathing configuration.

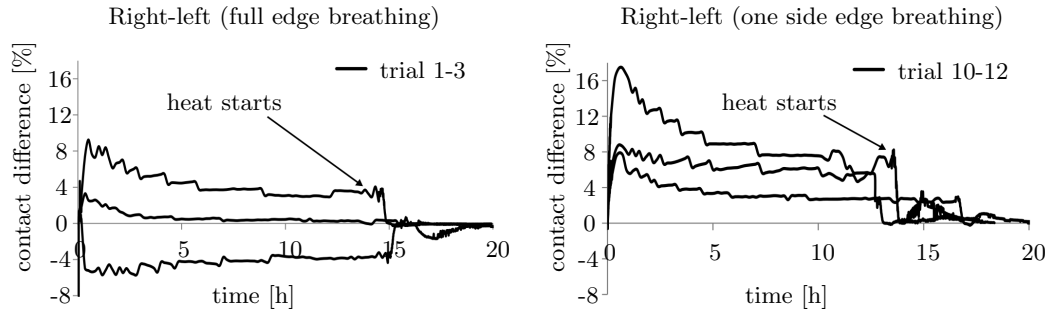

Figure 17: Comparison of the contact gradients in the full edge breathing and one sided edge breathing configurations.

for contact evolution along and across the fibre direction, in the x and y directions indentified in Fig. 3. For contact across the fibres (y-direction), pixel columns were averaged and for contact along the fibres (x-direction), pixel rows were averaged. Results along the fibre direction are shown in Fig. 18(a) for full edge breathing and Fig. 18(b) for sealed evacuation channels, meanwhile the contact along the fibre direction is shown in Fig. 18(c) and (d). Higher variability was observed across the fibres (in the y-direction) than along the fibres (in the x-direction) from Fig. 18(a) and (c) as well as Fig. 18(b) and (d). This variability reflects the air evacuation pattern of unidirectional prepregs. Interconnected valleys along the fibre direction serve as evacuation pathways and entrapped air impedes contact until heat is applied

to soften the resin, and enable a combination of resin and air flow. A direct

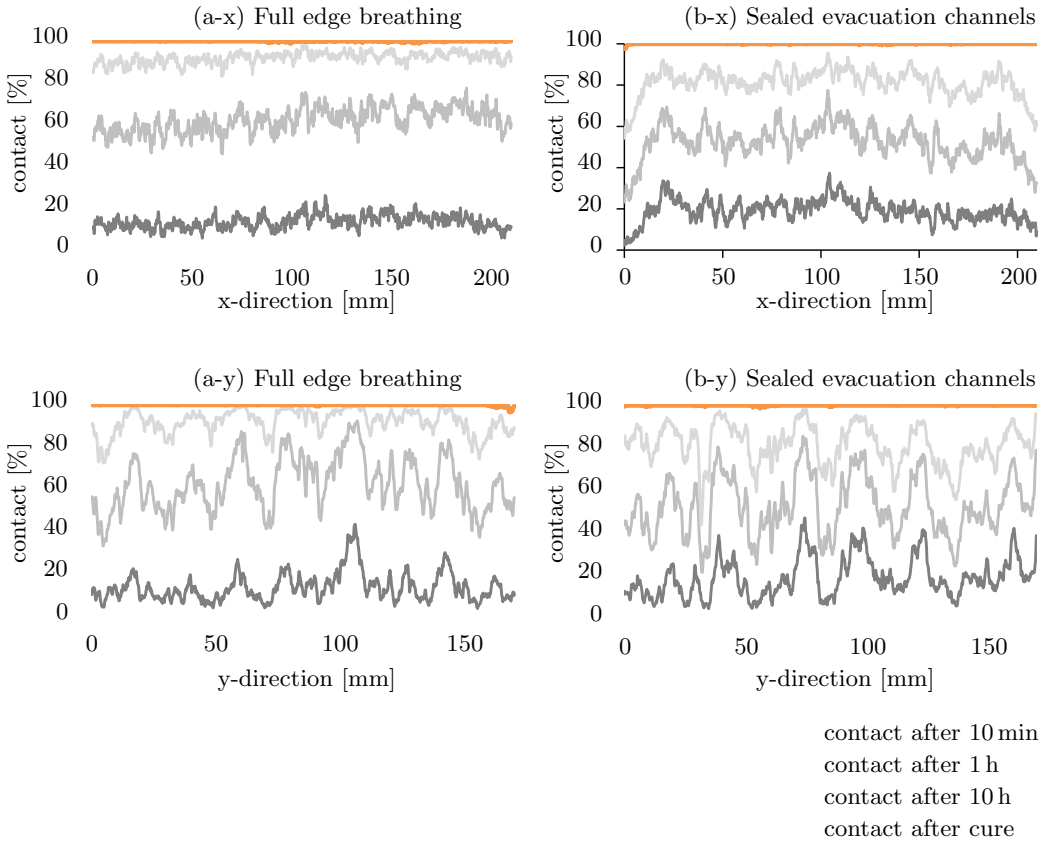

Figure 18: Contact in x- and y-directions for 10 minutes, 1 hour, 10 hours, and after heating.

comparison between the full edge breathing and sealed evacuation channels after 10 hours into the vacuum hold is shown in Fig. 19 to accentuate the difference in contact across the fibres between these two configurations. In general, the contact profile for sealed evacuation channels is rougher compared to the full edge breathing profile. Expanded non-contact areas are present, which is in agreement with wider white bands within the binary images (Fig. 8). This observation supports the assumption that air has to be evacuated between the glass tool-prepreg interface when the intraply air

evacuation channels of the prepreg are sealed. Accordingly, forcing air evacuation in the interply zone decreased the percentage of ply contact before heating.

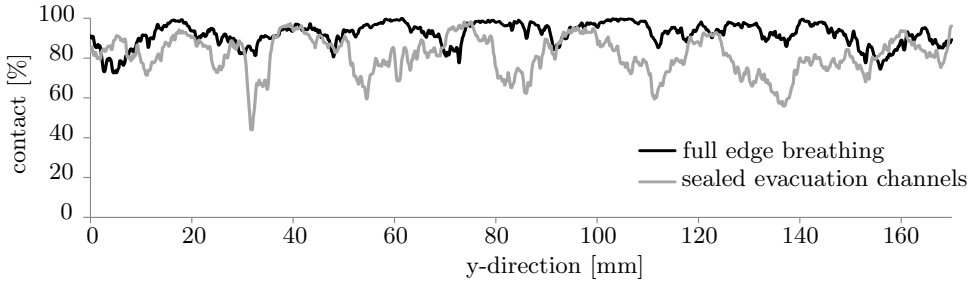

Figure 19: Contact in y-direction for full edge breathing and sealed evacuation channels after 10 hours into the ambient temperature vacuum hold.

5. Summary

In this paper, the surface of OoA prepregs was investigated in order to establish an understanding of air entrapment between plies. The contact evolution between a glass plate and a prepreg ply was measured during the consolidation process under various edge breathing conditions in order to identify the interply air evacuation mechanisms in unidirectional OoA prepregs.
The surface roughness of the prepreg ply was influenced by the nature of the unidirectional fibrebed: surface valleys form a corduroy texture along the fibre direction. As a result, contact was more pronounced along the fibre direction than across the fibres. Contact was observed to evolve from the initiation points into larger contact areas, instead of many smaller contact areas connecting. In fact, non-contact areas (considered to be interply voids) relocated into the valleys of the prepreg surface, and remained mostly visible throughout the ambient vacuum hold. These observations indicate that surface roughness valleys serve as interply air evacuation pathways for entrapped air.
In order to investigate the effect of a region of a ply becoming isolated from

the vacuum source during processing, the contact evolution of completely sealed plies was measured, and the results suggest that air relocates into the dry intraply region of partially saturated prepregs, and does not remain in the interply region. However, the variability in contact between repeats of the same test configuration suggests that local phenomena are likely to occur. This can be attributed to property variations within the prepreg: random resin and fibre volume fraction distributions influence the surface structure as well as the permeability in the in-plane and out-of-plane directions. The out-of-plane permeability determines the amount of entrapped air, whereas the in-plane air permeability mainly influences the evacuation time frame and the corresponding contact evolution.
A drop in contact at around 90 °C suggests that the contact evolution in the interply zone was not solely determined by air initially entrapped between plies, but is also affected by absorbed moisture, which was released by the material at elevated temperatures.
Overall, a test method was established to investigate the interaction of the phenomena that define the final part quality in regards to air entrapment between plies. The results presented here are an important first step towards a better understanding of the phenomena associated with the interply void formation in OoA prepregs. This study provides a basis for a more widespread analysis of interply void formation.

6. Acknowledgement

This work was conducted within the framework of a G8-2012 project on Material efficiency: A first step towards sustainable manufacturing between the University of Southern California, McGill University, the Technische Universität München, and the University of Bristol. Funding for this work was provided by the German Research Foundation (DFG) (contract number: DR 204/5-1) and the UK Engineering and Physical Science Research Council (EPSRC), under grant no. EP/K025023/1. We would like to acknowledge the Chair of Biomedical Physics at TUM for the acquisition of CT data,

Alicona UK Ltd. for the generation of surface roughness images and data, and Dr. Dominic Bloom for insightful discussions.

[1] Bloom D, Napper MA, Ward C and Potter K (2015) On the evolution of the distribution of entrapped air at the tool/first ply interf'ace during lay-up and debulk. *Advanced Manufacturing: Polymer & Composites Science* 1(1): 36–43.

[2] Centea T, Grunenfelder LK and Nutt SR (2015) A review of out-of-autoclave prepregs–material properties, process phenomena, and manufacturing considerations. *Composites Part A: Applied Science and Manufacturing* 70: 132–154.

[3] Centea T and Hubert P (2011) Measuring the impregnation of an out-of-autoclave prepreg by micro-ct. *Composites Science and Technology* 71(5): 593–599.

[4] Centea T and Hubert P (2013) Out-of-autoclave prepreg consolidation under deficient pressure conditions. *Journal of Composite Materials* (In Press).

[5] Farhang L and Fernlund G (26-28 September 2011) Void morphology, void evolution and gas transport in out-of-autoclave prepregs. In: *Proceedings of the 26th Annual Technical Conference of the American Society for Composites 2011, Montreal, QC, Canada.*

[6] Gadelmawla E, Koura M, Maksoud T, Elewa I and Soliman H (2002) Roughness parameters. *Journal of Materials Processing Technology* 123(1): 133–145.

[7] Garstka T, Ersoy N, Potter K and Wisnom M (2007) In situ measurements of through-the-thickness strains during processing of as4/8552 composite. *Composites Part A: Applied Science and Manufacturing* 38(12): 2517–2526.

[8] Grunenfelder L and Nutt S (2010) Void formation in composite prepregs–effect of dissolved moisture. *Composites Science and Technology* 70(16): 2304–2309.

[9] Gutowski TG, Cai Z, Bauer S, Boucher D, Kingery J and Wineman S (1987) Consolidation experiments for laminate composites. *Journal of Composite Materials* 21(7): 650–669.

[10] Hamill L, Centea T and Nutt S (2015) Surface porosity during vacuum bag-only prepreg processing: Causes and mitigation strategies. *Composites Part A: Applied Science and Manufacturing* 75: 1–10.

[11] Helmus R, Centea T, Hubert P and Hinterhölzl R (2015) Out-of-autoclave prepreg consolidation: Coupled air evacuation and prepreg impregnation modeling. *Journal of Composite Materials* : 0021998315592005.

[12] Helmus R, Hinterhölzl R and Hubert P (2015) A stochastic approach to model material variation determining tow impregnation in out-of-autoclave prepreg consolidation. *Composites Part A: Applied Science and Manufacturing* .

[13] Johnson KL (1987) *Contact Mechanics*. Cambridge University Press.

[14] Kardos JL, Duduković MP and Dave R (1986) Void growth and resin transport during processing of thermosettingmatrix composites. In: *Epoxy resins and composites IV*. Springer, pp. 101–123.

[15] Kratz J, Hsiao K, Fernlund G and Hubert P (2012) Thermal models for mtm45-1 and cycom 5320 out-of-autoclave prepreg resins. *Journal of Composite Materials* 47(3): 341–352.

[16] Kratz J and Hubert P (2013) Anisotropic air permeability in out-of-autoclave prepregs: Effect on honeycomb panel evacuation prior to cure. *Composites Part A: Applied Science and Manufacturing* 49: 179–191.

[17] Kratz J and Hubert P (2015) Vacuum bag only co-bonding prepreg skins to aramid honeycomb core. part i. model and material properties for core pressure during processing. *Composites Part A: Applied Science and Manufacturing* 72: 228–238.

[18] Lukaszewicz DHJA and Potter KD (2011) The internal structure and conformation of prepreg with respect to reliable automated processing. *Composites Part A: Applied Science and Manufacturing* 42(3): 283–292.

[19] Olivier P, Cottu JP and Ferret B (1995) Effects of cure cycle pressure and voids on some mechanical properties of carbon/epoxy laminates. *Composites* 26(7): 509–515.

[20] Persson BNJ, Albohr O, Tartaglino U, Volokitin AI and Tosatti E (2005) On the nature of surface roughness with application to contact mechanics, sealing, rubber friction and adhesion. *Journal of Physics: Condensed Matter* 17(1): R1.

[21] Ridgard C (18-21 May 2009) Out of autoclave composite technology for aerospace, defense and space structures. In: *Proceedings of the SAMPE Conference, Baltimore, MD, USA*. pp. 1–10.

[22] Tavares SS, Michaud V and Månson JAE (2009) Through thickness air permeability of prepregs during cure. *Composites Part A: Applied Science and Manufacturing* 40(10): 1587–1596.

[23] Zhang D, Heider D, Advani SG and Gillespie JW (6-9 May 2013) Out of autoclave consolidation of voids in continuous fiber reinforced thermoplastic composites. In: *Proceedings of the SAMPE Conference, Long Beach, CA, USA*. pp. 1–10.